Program Digest, 2019 IEEE International Ultrasonics Symposium (IUS)
Glasgow, Scotland, October 6-9, 2019

High contrast power Doppler imaging using intravascular ultrasound

Graham Collins
Joint Department of Biomedical Engineering
Georgia Institute of Technology
Atlanta, Georgia, USA
grahamcollins@gatech.edu

Bowen Jing
Joint Department of Biomedical Engineering
Georgia Institute of Technology
Atlanta, Georgia, USA
bowen.jing@bme.gatech.edu

Brooks Lindsey
Joint Department of Biomedical Engineering
Georgia Institute of Technology
Atlanta, Georgia, USA
brooks.lindsey@bme.gatech.edu

***Abstract*— The ability to predict likelihood of plaque rupture could be used to determine the course of treatment in coronary artery disease. One indicator of vulnerability is intra-plaque neovascularization, the development of blood vessels within plaque. In order to visualize these vessels with rotational, side-viewing intravascular ultrasound (IVUS), a new approach for imaging blood flow in small vessels is proposed based on compounding adjacent angular acquisitions. This approach was evaluated in tissue mimicking phantoms and *ex vivo* porcine vessels using both conventional and singular value decomposition (SVD) filtering. Flow was imaged at a rate of 5.6 mm/s in 200 µm tubes adjacent to the lumen of *ex vivo* porcine arteries to mimic microvessels. As a result of compounding, the Doppler CNR increased from 5.3 ± 0.95 to 7.2 ± 1.3 (conventional filtering) and from 23 ± 3.3 to 32 ± 6.7 (SVD filtering). Applying these strategies could allow increased sensitivity to slow flow in side-viewing intravascular ultrasound imaging.**

Keywords—intravascular ultrasound, functional imaging, SVD filter, plaque characterization, compounding

I. Introduction

Coronary artery disease is a leading cause of mortality globally (13.2% of deaths as of 2012) according to the World Health Organization [1]. The ability to stratify risk of plaque rupture could reduce rates of Major Adverse Cardiac Events (MACE) by determining which lesions would benefit from intervention (e.g. stenting). Vasa vasorum are small vessels (~70 to 500 µm in diameter) that supply the wall of the coronary artery with nutrients [2, 3]. During plaque development, vasa vasorum grow from the adventitial layer into the plaque itself (intra-plaque neovascularization). The density of vasa vasorum within the plaque has been demonstrated to be correlated with severity of stenosis in humans [4] and with plaque vulnerability in animal models of atherosclerosis [5, 6].

Current intravascular flow imaging techniques are challenged to identify slow blood flow in the small vessels of the vasa vasorum due to the difficulty of separating signals arising from slow blood flow from surrounding higher amplitude tissue signals having motion rates similar or higher than the flow rates [3].

This work was supported by the Department of Biomedical Engineering and the College of Engineering at Georgia Institute of Technology and by R01HL144714 from the National Institute of Health.

When imaging blood flow within vasa vasorum using 2D rotational IVUS, there will be components in the imaging plane as well as out-of-plane flow, resulting in new scatterers entering the imaging plane on each successive measurement. However, by effectively filtering stationary or slow-moving structures observed on subsequent rotations, it is possible to form images that localize blood flow, analogous to power Doppler images in ultrasound imaging with array transducers [7].

We present approaches for increasing sensitivity to blood flow in mechanically-steered IVUS imaging by compounding wall-filtered data from adjacent angles. In array-based ultrasound, compounding is commonly used to improve the point spread function and thus increase contrast, spatial resolution, and signal-to-noise ratio (SNR) [8, 9]. In this work, angular compounding to increase flow sensitivity in mechanically-steered IVUS data is demonstrated with both conventional and SVD clutter filters. The sensitivities of these processing approaches are evaluated in tissue-mimicking phantoms with introduced motion and in *ex vivo* porcine arteries.

II. Materials and Methods

A. Determination of compounding angle

Compounding is applied to increase SNR; however, an excessively large compounding angle leads to summation of decorrelated signals and results in decreased SNR. Conversely, compounding over an angular extent that is too narrow fails to realize the maximum SNR improvement. Angular correlation in rotational IVUS was investigated using two custom tissue mimicking phantoms: one containing only diffuse targets (α=0.5 dB/cm/MHz, $SNR_{speckle} = 1.68 \pm 0.06$) [10], and a second phantom containing a 140 µm wire embedded in diffuse scatterers (α=0.5 dB/cm/MHz). Radiofrequency (RF) echo data were acquired from this phantom using the setup described below.

RF data were bandpass filtered with a 4th order Butterworth filter (14-28 MHz) and upsampled to 400 MHz. In order to assess angular correlation, the normalized correlation coefficient was computed [11] as a function of angle for 1 mm segments of acquired RF lines centered at depths varying from 2-30 mm. For each depth, the angular extent for compounding

was determined based on the maximum angular extent for which $\rho \geqslant 0.5$ for windowed RF data.

B. Transducer and data acquisition system

Radiofrequency (RF) echo data were acquired using a custom laboratory IVUS system with a 1.1 x 0.55 mm, side-viewing 20 MHz transducer [12]. The transducer was mounted on a stepper motor (step size: 0.225°) controlled by a microcontroller (Arduino UNO, Torino, Italy). At each angular position, the transducer was excited by a negative impulse with a peak amplitude of -227 volts (Panametrics 5900PR, Waltham, MA, USA), then radiofrequency (RF) data were digitized at a sampling rate of 100 MHz (PDA14, Signatec, Corona, CA) using a custom program (LabVIEW, National Instruments Corp., Austin, TX). During data acquisition, the transducer was moved relative to the phantom using a 3-axis motion stage (Newport XPS, Irvine, CA) to simulate physiological motion. After each rotation, the transducer was translated by 1 mm in the elevation direction by the motion stage to provide 3D data. The slow time period between subsequent acquisitions at the same spatial position was ~33 seconds to allow a full rotation.

C. Motion Correction

Due to the low acquisition rate relative to flow rate, motion correction is needed between acquisitions to align acquired data in the presence of simulated tissue motion. In this work, acquired 2D frames were aligned using a local block matching method similar to the method previously described in [13]. Briefly, 2D block matching was used with relatively large kernels (6.8 mm x 2.25°) and a search region of 7 mm x 4.5° to determine the delays maximizing cross-correlation between all adjacent frames. False matches were reduced by limiting the search region to velocities less than 20 μm/s, or 2 mm per 30 frame ensemble. After curve fitting to prevent discontinuities [14, 15], for each frame, entire lines of acquired RF data were aligned with respect to the central frame (e.g. frame 15 for an ensemble size of 30).

D. Power Doppler processing

In order to form power Doppler images, acquired RF data were bandpass filtered with a 4th order Butterworth filter (14-28 MHz) and upsampled to 400 MHz, then motion correction was performed as described previously. Next, one of four different post-processing strategies was applied to form the power Doppler images: A) Butterworth high pass filtering without angular compounding, B) SVD filtering without angular compounding, C) Butterworth high pass filtering with angular compounding, and D) SVD filtering with angular compounding. An ensemble size of 30 frames was used. All processing was performed in Matlab (The Mathworks, Natick, MA, USA).

For Butterworth filtering schemes, motion-corrected RF data were filtered in slow time to remove slow-moving tissue echoes, and the complex envelope was estimated. Frequency cutoffs of 3 and 12 mHz were used, analogous to approximately 3 and 12 kHz in real-time IVUS imaging acquiring at 30 revolutions per second.

For SVD filtering, each angular location from the cross section was filtered individually to ensure high local spatial correlation. The first two singular values were observed to correspond to tissue signals with high correlation in slow time and thus were discarded. For cases (C) and (D) with compounding, envelope-detected data were compounded over the number of angular acquisitions for which ρ exceeded 0.5 in preliminary experiments in tissue speckle-producing phantoms as described previously. Filter parameters were held constant through all experiments.

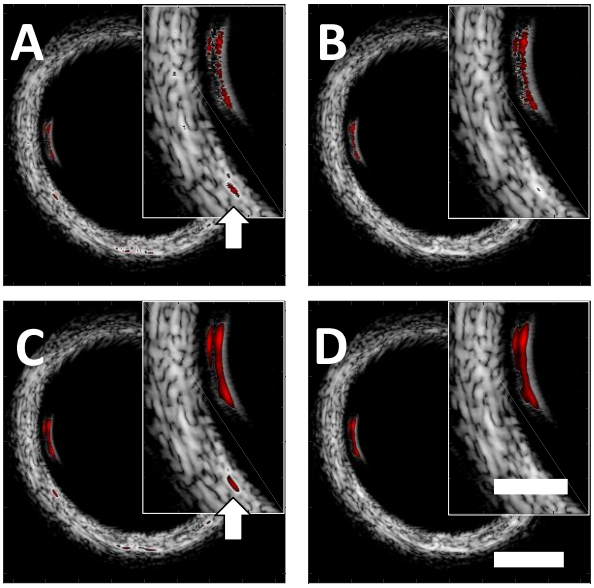

Fig. 1. Motion-corrected power Doppler data (red) overlaid on B-mode data (grayscale) for a 200 μm tube positioned adjacent to the inner surface of a 7 mm *ex vivo* porcine vessel for images formed via A) Butterworth, B) SVD, C) Butterworth with compounding, and D) SVD with compounding. Power Doppler data are displayed with 5 dB dynamic range, and B-mode is displayed with 35 dB dynamic range. The arrows denote residual tissue signal above 5 dB that is misclassified as flow. The insets show magnifed versions of the region of interest. The primary scale bar indicates 2 mm, and the scale bar for the inset indicates 1 mm.

E. Acquisition of flow imaging data

An excised porcine carotid artery (Sierra Medical, Whittier, CA) was held in a custom frame under tension, and 200 μm-diameter cellulose tubing (Spectrum Labs, Rancho Dominguez, CA, USA) was positioned adjacent to the inner wall of the lumen parallel to the long axis of the vessel to mimic a microvessel. The distance from the transducer to the vessel wall and adjacent cellulose tubing was approximately 4 mm. 10^8 microbubbles / mL were infused in the 200 μm tube at a rate of 5.6 mm/s (PHD2000, Harvard Apparatus, Holliston, MA). While the goal is ultimately to image blood flow with high sensitivity without the use of exogenous contrast agents, perfluorobutane microbubbles were used in initial studies to provide a scattering source with a controllable amplitude [16]. 3D data sets were acquired by translating the transducer in the

elevation direction with a step size of 1 mm. RF data were processed independently slice-by-slice as described (see section "Power Doppler processing").

In parallel, data was acquired with flow in a cellulose tube embedded in a tissue-mimicking phantom (α=0.5 dB/cm/MHz). During data acquisition, the transducer was moved linearly relative to the phantom in the imaging plane at a rate of 6.6 µm/s, or 0.66 mm per 30 frame ensemble to mimic physiological motion that occurs during imaging [17]. This velocity is similar to tissue motion in the case of the left anterior descending coronary artery during the cardiac cycle [18].

For each processing approach, the effectiveness of flow imaging was quantified by computing the Doppler CNR [19]:

$$CNR_{Doppler} = \frac{\overline{PW_{flow}} - \overline{PW_{tissue}}}{std(PW_{tissue})}, \quad (1)$$

Where PW_{flow} and PW_{tissue} represent the magnitude of the Doppler data regions of flow and tissue, respectively, and overbar denotes mean. Significance of observed differences in Doppler CNR with and without compounding was assessed using paired t-tests with an alpha level of 0.05. Additionally, 3D projections of imaging data were created in ImageJ by displaying the brightest point.

III. Results

A. Determination of compounding angle

The preliminary study revealed that correlation as a function of angle [20] remains close to one for the coherent target over an angular extent of six degrees. For the diffuse case, the correlation coefficient decreases more rapidly as a function of angular rotation. For each axial (depth) window, acquisitions for which the correlation coefficient remains $\geq$ 0.5 were compounded in subsequent experiments.

B. Flow imaging data

Images of flow in a 200 µm tube positioned on the inner surface of an porcine artery are shown in Fig. 1. The maximum backscattered amplitude from the vessel wall in B-mode was 15 dB greater than the maximum amplitude from flow within the tube, and the mean backscattered amplitude was > 6 dB higher in the wall of the *ex vivo* vessel than in the region of flow. Fig. 1A and Fig. 1C contain residual vessel wall signal visible in images formed with Butterworth filtering. Images formed with SVD filtering do not have visible vessel wall signal above 5 dB. For both Butterworth and SVD filtering, compounded images have a larger, more contiguous flow area above the display threshold. Additionally, compounding resulted in increased visibility of flow in the tube. Doppler CNR values were 5.3 ± 0.95 (Butterworth, no compounding), 7.2 ± 1.3 (Butterworth, with compounding), 23 ± 3.3 (SVD, no compounding), 32 ± 6.7 (SVD, with compounding), as presented in Fig. 2. Paired *t*-tests indicate significant increases in Doppler CNR due to compounding (p=4.8 x 10^{-5} for Butterworth and p=0.0036 for SVD).

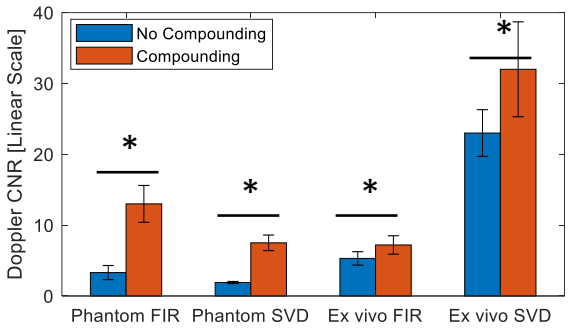

Fig. 2. Doppler CNR for Butterworth and SVD filtering without (blue) and with compounding (orange) for flow in a 200 µm tube in a tissue-mimicking phantom or on the inner surface of a 7 mm-diameter *ex vivo* porcine artery. The asterisks denote statistical significance using paired t-tests with alpha level of 0.05.

In phantom studies, the area of false flow artifact outside of the region of flow is smaller than in the non-compounded images. Qualitatively, the compounded images show larger regions of flow above the display threshold. For Butterworth filtering, Doppler CNR increases from 3.3 ± 1.0 to 13 ± 2.6 due to compounding. For SVD filtering Doppler CNR increases from 1.9 ± 0.15 to 7.5 ± 1.1 due to compounding, as illustrated in Fig. 2. Paired *t*-tests indicate significant increases in Doppler CNR due to compounding (p=0.0099 for Butterworth and p=0.014 for SVD).

Finally, 3D views of the porcine artery with overlaid flow from SVD filtering with compounding are shown in Fig. 3. The grayscale image reveals the morphology of the vessel wall, while the flow within the tube is observed in the overlaid flow image.

IV. Discussion

By compounding adjacent angular acquisitions with $\rho \geqslant 0.5$, a statistically significant increase in Doppler CNR was observed for each filter and imaging scenario. The increased SNR due to compounding correlated echoes results in an increase in sensitivity to slow-moving flow. While the current work used a relatively large, lower frequency transducer, in the case of a smaller, higher frequency transducer for coronary imaging, a smaller angular step size might be necessary, i.e. a higher PRF for a continuously rotating system.

Results indicated that SVD filtering provided superior separation of flow relative to the Butterworth filter in a mixed tissue environment containing both coherent and diffuse regions. This finding is consistent with reports that the SVD filter can separate bright targets based on slow time correlation that conventional frequency-based filters are not able to suppress [19]. In the case of the *ex vivo* vessel, the flow in the microtube was proximal to the tissue, i.e. there is little attenuation between the transducer and flow relative to the phantom case. The observed improvements in Doppler CNR due to compounding in the artery case were approximately 38% for both Butterworth and SVD filtering, and Doppler CNR values increased by approximately a factor of four due to compounding. The decreased improvement in Doppler CNR

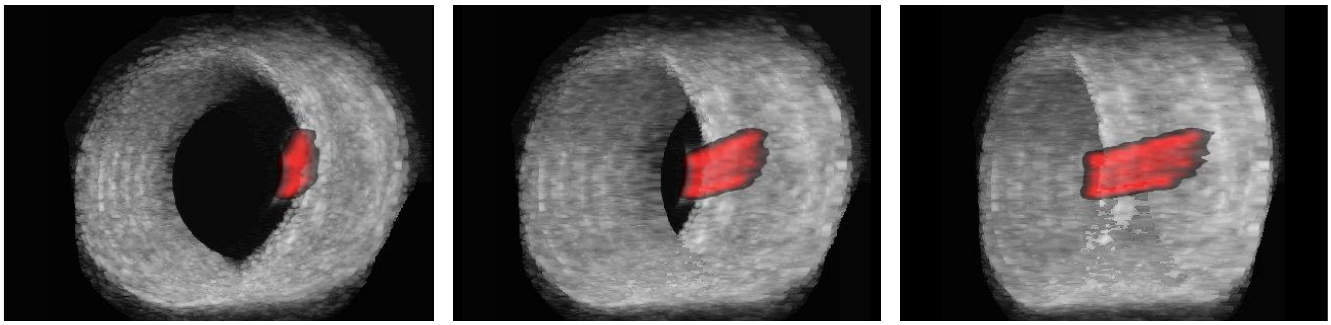

Fig. 3. Motion-corrected power Doppler data (red) overlaid on B-mode data (grayscale) for a 200 μm tube positioned adjacent to the inner surface of a 7 mm *ex vivo* porcine vessel for images formed via SVD filtering with angular compounding.

relative to the improvement in the phantom experiments was likely the result of higher SNR without compounding due to the described lower attenuation. Clinically, the blood flow signals would be attenuated by both blood in the lumen and by the intima.

V. Conclusion

Intraplaque vasa vasorum are challenging to visualize using IVUS due to the difficulty of detecting slow flow in small vessels in the presence of tissue motion. Applying angular compounding between adjacent angular acquisitions increased sensitivity to flow in small vessels with slow flow in experimental setups. When imaging flow at 5.6 mm/s in 200 μm tubes adjacent to the lumen of ex vivo porcine arteries, the Doppler CNR increased from 5.3 ± 0.95 to 7.2 ± 1.3 for Butterworth and from 23 ± 3.3 to 32 ± 6.7 for SVD filtering. In imaging the porcine artery, flow was visualized even though the maximum backscattered amplitude of the vessel wall was 15 dB greater than that of flow within the tube. Translating these benefits to a high-rotation rate system could improve the ability to assess plaque vulnerability and guide clinical decisions, such as determining which lesions require intervention in patients with stable disease.

References

[1] McAloon, Christopher J., et al. "The changing face of cardiovascular disease 2000–2012: An analysis of the world health organisation global health estimates data." International journal of cardiology 224: 256-264, Dec. 2016.

[2] R. Puri, M. I. Worthley, and S. J. Nicholls, "Intravascular imaging of vulnerable coronary plaque: current and future concepts," Nature Reviews Cardiology, vol. 8, no. 3, pp. 131–139, Mar. 2011.

[3] A. Redwood, D. R. H. Iii, and R. Robb, "Using ChromaFlo intra-vascular ultrasound (IVUS) to analyze adventitial vasa vasorum distribution: Considerations and recommendations," in Progress in Biomedical Optics and Imaging - Proceedings of SPIE, 2006, p. 614309.

[4] M. Kumamoto, Y. Nakashima, and K. Sueishi, "Intimal neovascularization in human coronary atherosclerosis: Its origin and pathophysiological significance," Human Pathology, vol. 26, no. 4, pp. 450–456, Apr. 1995.

[5] Langheinrich Alexander C. et al., "Correlation of Vasa Vasorum Neovascularization and Plaque Progression in Aortas of Apolipoprotein E−/−/Low-Density Lipoprotein−/− Double Knockout Mice," Arteriosclerosis, Thrombosis, and Vascular Biology, vol. 26, no. 2, pp. 347–352, Feb. 2006.

[6] T.-G. Kwon, L. O. Lerman, and A. Lerman, "The Vasa Vasorum in Atherosclerosis: The Vessel Within the Vascular Wall," Journal of the American College of Cardiology, vol. 65, no. 23, pp. 2478–2480, Jun. 2015.

[7] J. R. Crowe and M. O'Donnell, "Quantitative blood speed imaging with intravascular ultrasound," IEEE Transactions on Ultrasonics, Ferroelectrics, and Frequency Control, vol. 48, no. 2, pp. 477–487, Mar. 2001.

[8] G. Montaldo, M. Tanter, J. Bercoff, N. Benech, and M. Fink, "Coherent plane-wave compounding for very high frame rate ultrasonography and transient elastography," IEEE Transactions on Ultrasonics, Ferroelectrics, and Frequency Control, vol. 56, no. 3, pp. 489–506, Mar. 2009.

[9] B. Denarie et al., "Coherent Plane Wave Compounding for Very High Frame Rate Ultrasonography of Rapidly Moving Targets," IEEE Transactions on Medical Imaging, vol. 32, no. 7, pp. 1265–1276, Jul. 2013.

[10] E. L. Madsen, J. A. Zagzebski, R. A. Banjavie, and R. E. Jutila, "Tissue mimicking materials for ultrasound phantoms," Medical Physics, vol. 5, no. 5, pp. 391–394, 1978.

[11] M. E Anderson and G. Trahey, "A seminar on k -space applied to medical ultrasound," Aug. 2019.

[12] B. D. Lindsey, J. Kim, P. A. Dayton, and X. Jiang, "Dual-Frequency Piezoelectric Endoscopic Transducer for Imaging Vascular Invasion in Pancreatic Cancer," IEEE Transactions on Ultrasonics, Ferroelectrics, and Frequency Control, vol. 64, no. 7, pp. 1078–1086, Jul. 2017.

[13] K. Y. E. Leung, R. A. Baldewsing, F. Mastik, J. A. Schaar, A. Gisolf, and A. F. W. van der Steen, "Motion compensation for intravascular ultrasound palpography," IEEE Transactions on Ultrasonics, Ferroelectrics, and Frequency Control, vol. 53, no. 7, pp. 1269–1280, Jul. 2006.

[14] S. G. Foster, P. M. Embree, and W. D. O'Brien, "Flow velocity profile via time-domain correlation: error analysis and computer simulation," IEEE Transactions on Ultrasonics, Ferroelectrics, and Frequency Control, vol. 37, no. 3, pp. 164–175, May 1990.

[15] G. C. Ng, S. S. Worrell, P. D. Freiburger, and G. E. Trahey, "A comparative evaluation of several algorithms for phase aberration correction," IEEE Transactions on Ultrasonics, Ferroelectrics, and Frequency Control, vol. 41, no. 5, pp. 631–643, Sep. 1994.

[16] B. D. Lindsey et al., "High Resolution Ultrasound Superharmonic Perfusion Imaging: *In Vivo* Feasibility and Quantification of Dynamic Contrast-Enhanced Acoustic Angiography," Ann Biomed Eng, vol. 45, no. 4, pp. 939–948, Apr. 2017.

[17] Yan Shi, F. J. de Ana, S. J. Chetcuti, and M. O'Donnell, "Motion artifact reduction for IVUS-based thermal strain imaging," IEEE Transactions on Ultrasonics, Ferroelectrics, and Frequency Control, vol. 52, no. 8, pp. 1312–1319, Aug. 2005.

[18] B. Lu et al., "Coronary Artery Motion During the Cardiac Cycle and Optimal ECG Triggering for Coronary Artery Imaging," Investigative Radiology, vol. 36, no. 5, p. 250, May 2001.

[19] C. Demené et al., "Spatiotemporal Clutter Filtering of Ultrafast Ultrasound Data Highly Increases Doppler and fUltrasound Sensitivity," IEEE Transactions on Medical Imaging, vol. 34, no. 11, pp. 2271–2285, Nov. 2015.

[20] R. Mallart and M. Fink, "The van Cittert–Zernike theorem in pulse echo measurements," The Journal of the Acoustical Society of America, vol. 90, no. 5, pp. 2718–2727, Nov. 1991.